Journal for ImmunoTherapy of Cancer

Spatial transcriptomics of macrophage infiltration in non-small cell lung cancer reveals determinants of sensitivity and resistance to anti-PD1/PD-L1 antibodies

Mathieu Larroquette,[1,2] Jean-Philippe Guegan,[3] Benjamin Besse,[4] Sophie Cousin,[1] Maxime Brunet,[1,2] Sylvestre Le Moulec,[5] François Le Loarer,[6] Christophe Rey,[3] Jean-Charles Soria,[4] Fabrice Barlesi,[4] Alban Bessede,[3] Jean-Yves Scoazec,[7] Isabelle Soubeyran,[6] Antoine Italiano [1,2,8]

To cite: Larroquette M, Guegan J-P, Besse B, *et al*. Spatial transcriptomics of macrophage infiltration in non-small cell lung cancer reveals determinants of sensitivity and resistance to anti-PD1/PD-L1 antibodies. *Journal for ImmunoTherapy of Cancer* 2022;**10**:e003890. doi:10.1136/jitc-2021-003890

► Additional supplemental material is published online only. To view, please visit the journal online (http://dx.doi.org/10.1136/jitc-2021-003890).

ML and J-PG contributed equally.

Accepted 22 February 2022

For numbered affiliations see end of article.

Correspondence to
Dr Antoine Italiano;
a.italiano@bordeaux.unicancer.fr

ABSTRACT

Background Tumor-associated macrophages (TAMs) having immunosuppressive properties are one of the most abundant immune cells in the tumor microenvironment (TME). Preclinical studies have highlighted the potential role of TAMs in resistance to immune checkpoint blockers (ICBs). Here, we investigated the predictive value of TAM infiltration in patients with non-small cell lung cancer (NSCLC) treated with ICBs and characterized their transcriptomic profiles.

Methods Tumor samples were collected from 152 patients with NSCLC before ICB treatment onset. After immunohistochemical staining and image analysis, the correlation between CD163+ cell infiltration and survival was analyzed. Spatial transcriptomic analyses were performed using the NanoString GeoMx Immune Pathways assay to compare the gene expression profile of tumors with high or low levels of CD163+ cell infiltration and to identify determinants of response to ICBs in tumors with high CD163+ infiltration.

Results Low intratumoral CD163+ cell infiltration was associated with longer progression-free survival (PFS; HR 0.61, 95% CI 0.40 to 0.94, p=0.023) and overall survival (OS; HR 0.48, 95% CI 0.28 to 0.80, p=0.004) under ICB treatment. Spatial transcriptomic profiles of 16 tumors revealed the upregulation of *ITGAM*, CD27, and *CCL5* in tumors with high CD163+ cell infiltration. Moreover, in tumors with high macrophage infiltration, the upregulation of genes associated with the interferon-γ signaling pathway and the M1 phenotype was associated with better responses under immunotherapy. Surprisingly, we found also a significantly higher expression of *CSF1R* in the tumors of responders. Analysis of three independent data sets confirmed that high *CSF1R* expression was associated with an increased durable clinical benefit rate (47% vs 6%, p=0.004), PFS (median 10.89 months vs 1.67 months, p=0.001), and OS (median 23.11 months vs 2.66 months, p<0.001) under ICB treatment.

Conclusions Enrichment of TAMs in the TME of NSCLC is associated with resistance to immunotherapy regardless of the programmed death ligand 1 status and is driven by upregulation of *CD27*, *ITGAM,* and *CCL5* gene expression within the tumor compartment. Our transcriptomic analyses identify new potential targets to alter TAM recruitment/polarization and highlight the complexity of the CSF1R pathway, which may not be a suitable target to improve ICB efficacy.

BACKGROUND

Immune checkpoint blockers (ICBs) have revolutionized the management of patients with non-small cell lung cancer (NSCLC). Blocking the interaction between the programmed cell death protein 1 (PD-1) receptor and its primary ligand (PD-L1) has demonstrated remarkable anticancer activity, and anti-PD-1/PD-L1 drugs have been approved both as single agents or in combination with cytotoxic chemotherapy.[1 2] However, most patients receiving anti-PD-1/PD-L1 monoclonal antibodies do not derive benefit.[2] Hence, there is a crucial need to identify reliable predictive biomarkers of the response to anti-PD-1/PD-L1 agents to develop precision medicine for NSCLC immunotherapy[3 4] as well as to identify novel mechanisms underlying resistance to ICBs.

Thus far, PD-L1 expression status as assessed by immunohistochemistry (IHC) is the sole companion diagnostic marker approved both in the USA and in Europe to guide anti-PD1 therapy in patients with NSCLC.[4] However, as observed for many tumor types, PD-L1 expression is an imperfect predictor of a patient's response to immune checkpoint inhibition.[4]

In addition to CD8+ T cells, other immune cell populations may impact the efficacy of anti-PD1/PD-L1 antibodies. Several studies have shown that tumor-associated macrophages (TAMs) are one of the most abundant immune cells in the tumor microenvironment (TME) and are associated with poor disease prognosis in many tumor types.[5 6] It has been shown that TAMs carry

out immunosuppressive functions by inhibiting cytotoxic T lymphocyte (CTL) function in different ways, including the production of anti-inflammatory cytokines, metabolic activity with arginine uptake and the production of radical oxygen species, or even PD-L1 expression on their surface.[7–9] Interestingly, preclinical studies have highlighted the potential role of TAMs in resistance to ICBs.[10]

Our study aimed to investigate the predictive value of TAM infiltration in patients with NSCLC treated with ICBs and characterize their transcriptomic profile to decipher the impact of their heterogeneity on sensitivity to immunotherapy.

METHODS

Patients and study assessments

Retrospective data were collected from the medical records of 152 patients with NSCLC treated at three distinct sites: two academic centers (Institut Bergonié, Bordeaux, France, and Gustave Roussy, Villejuif, France) and one community hospital (Clinique Marzet, Pau, France). Patients from Institut Bergonié (n=80) and Gustave Roussy (n=39) were prospectively enrolled in the BIP (NCT02534649) and MATCH-R (NCT02517892) molecular profile screening programs, respectively. All included patients needed to have received ICB treatment for histologically proven advanced non-squamous or squamous NSCLC. Availability of paraffin-embedded tissue sections from the tumor before ICB administration was also required. All patients were treated at the discretion of their physician, in agreement with the current European Society of Medical Oncology guidelines.[11] Immunotherapy was administered either via standard therapy protocols or as part of a clinical trial. All responses to ICBs were assessed using the Response Evaluation Criteria in Solid Tumors guidelines.[12] Durable clinical benefit (DCB) was defined as the proportion of patients achieving objective response or stable disease lasting ≥12 months. Progression-free survival (PFS) was defined as the time from the start of treatment until disease progression, death, or last patient contact. Overall survival (OS) was defined as the time from the start of treatment until death or last patient contact.

Immunohistochemical staining and slide digitization

Immunohistochemical analysis was performed on the automated Ventana Discovery XT staining platform (Ventana Medical Systems). Slides of tumor tissue were deparaffinized in xylene and hydrated in serial alcohol solutions. Antigen retrieval was performed by the heat-induced epitope retrieval method. The slides were then incubated with the following primary antibodies: anti-CD8 (clone C8/144B, Dako) for CTLs, anti-CD163 (clone 10D6, Leica) for TAM, and anti-CK7 (SP52, Novus) for tumor cells. Bound primary antibodies were detected using either OmniMap anti-Ms or Rb-HRP together with DISCOVERY Green, Purple or 3,3'-diaminobenzidine (DAB) chromogen detection kit (Roche). The slides were counterstained with hematoxylin (Roche), cover-slipped, and finally digitized using a multispectral imaging platform (PhenoImager HT, Akoya). The acquired multispectral images were then used for further tissue annotation and image analysis.

Pathological evaluation

On each stained slide, the region containing tumor tissue and stroma was assessed and selected by a trained pathologist (IS) for subsequent analysis. Then, stained slides were analyzed via the InForm image analysis software (Akoya, V.2.4.1) to segment tissue into tumor and stroma and phenotype the CD8+ and CD163+ cells. Cell densities were finally computed in R using the PhenoptrReports package (V.0.2.8).

PD-L1 evaluation

The PD-L1 status of tumor samples was determined using tumor proportion score (TPS) obtained via immunostaining with the QR1 antibody (Diagomics). A positive PD-L1 status was defined as the presence of PD-L1 cytoplasmic labeling on at least 1% of the tumor cells.

Spatial transcriptomics

For spatial transcriptomic analyses, 16 patients with available chirurgical formalin-fixed, paraffin-embedded (FFPE) specimen were selected based on their level of CD163+ cell infiltration: eight patients with CD163+ cell tumor infiltration <470 cells/mm² (low) and eight patients with CD163+ cell tumor infiltration >470 cells/mm² (high). Briefly, 5 µm FFPE tissue sections mounted on positively charged slides were processed on the Ventana Discovery Ultra platform (Ventana, Roche Diagnostics). Slides were deparaffinized and target retrieval was performed. Next, tissues were washed and incubated with 2 µg/mL proteinase K in phosphate-buffered saline for 16 min at 37°C. Tissues were then fixed, washed, and incubated overnight at 37°C with GeoMx Immune Pathways Panel probes in a HybEZ II System oven.[13] Following incubation, tissues were washed twice and then incubated for 30 min at room temperature in a humidity chamber with saturation buffer (Buffer W, NanoString) prior to staining for 1 hour at room temperature with fluorescent-labeled CD45 and PanCK antibodies together with 100 µM SYTO.[13] Eleven to twelve regions of interest (ROIs) were selected across the whole slide in mixed stroma/tumor regions. These ROIs were selected as representative parts of the tumor. The ROIs were further segmented based on the PanCK staining to differentiate tumor versus stroma areas. After ultraviolet illumination, barcodes were collected in 96-well plates and dried for 1 hour at 65°C. Photocleaved oligos were resuspended in 10 µL nuclease-free water and hybridized to GeoMX Hyb codes at 65°C for 18 hours. Samples were finally pooled and processed on the nCounter MAX system (NanoString). nCounter counts were converted to digital count conversion file using the NanoString's GeoMx NGS pipeline (V.2.1) and imported back in the GeoMx Digital Spatial Profiler

(DSP) platform to generate an expression count matrix. After ROI quality control (QC) according to NanoString's recommendations and principal component analysis to eliminate potential outliers, areas of illumination (AOI) raw counts were normalized using full quantile normalization (limma R package V.3.46) and differential gene expression were tested using limma and adjusting p values using Benjamini-Hochberg correction. To account for the multiple ROIs per sample, the slide ID was used as a blocking factor. Heatmaps were generated using the pheatmap R package (V.1.0.12) after averaging the gene expression of the indicated AOIs per patient.

RNAseq analysis

RNA sequencing (RNAseq) data from 49 patients with NSCLC included in the MATCH-R (NCT02517892) study were analyzed, 39 of them had also FFPE sample available for IHC (online supplemental table 1). RNA seq was performed as previously described.[14] Briefly, reads were aligned to the hg38 human genome assembly using Rsubread (V.2.2.6) without prior trimming. Counts were then summarized at the gene level using FeatureCounts and normalized using Deseq2 (V.1.30.1).

Single-cell RNAseq analysis scRNAseq analysis was performed using Loupe Cell Browser (V.5.1.0) on the publicly available human NSCLC data set from 10× Genomics (https://support.10xgenomics.com/single-cell-gene-expression/datasets). CD68, CD163, and CSF1R positive cells were identified using an expression cut-off of 2.0.

Survival analysis from public data set

Level3 RSEM genes normalized data from the The Cancer Genome Atlas (TCGA) LUAD cohort were download from the Broad GDAC firehose (January 28 2016) and gene expression were log2(x+1) transform before performing survival analysis.

Normalized data for the GSE93157 (housekeeping gene normalization)[15] and for the GSE136961 (transcripts per million (TPM) value)[16] were downloaded from the GEO database and the lung cancer data were extracted.

Statistical analysis

PFS and OS were estimated using the Kaplan-Meier method. Patients were classified as 'high' or 'low' for their tumor or stroma cell infiltration (CD8+ or CD163+) as assessed by IHC. Classification was based on an optimized threshold obtained through the maximally selected rank statistics from the 'maxstat' R package and using the PFS as optimal outcome and 20% as the minimum proportion of observations per group (survminer R package V.0.4.9).

Survival differences between groups were assessed using the log-rank test (Survival R package V.3.2–13). The Cox proportional-hazards regression model was used to estimate HRs and 95% CIs. Multivariate analyses were performed using the survival Analysis R package (V.0.2.0). All the statistical analyses were carried out using R software (V.4.0.4).

RESULTS

CD8+ and CD163+ cell infiltration and response to ICBs

Using image analysis and a machine-learning approach, we analyzed the tumor samples of 152 patients with lung cancer obtained before treatment onset with an anti-PD1/PD-L1 agent to determine the density of CD8+ and CD163+ cells in both tumor and stroma areas (figure 1A and online supplemental figure 1). The main clinical and pathological characteristics of the patients are summarized in table 1.

The intratumoral median density for CD8+ T cells was 99 cells/mm^2 (range 0–2254). Using the survminer R package, we determined a cut-off value of 356 cells/mm^2 to define high-infiltrated tumors (>356/mm^2) and low-infiltrated tumors (≤356/mm^2) (online supplemental figure 2A). In the stroma, the median CD8+ T cells density was 328 cells/mm^2 (7–2894) and an optimal cut-off value of 697 cells/mm^2 was used to classify patients with high-infiltrated tumors (>697/mm^2) and low-infiltrated tumors (≤697/mm^2 infiltrated tumors) infiltrated tumors (online supplemental figure 2B).

The intratumoral median density for CD163+ cells was 1197 cells/mm^2 (range 0–10073). A cut-off value of 472 cells/mm^2 to define high-infiltrated tumors (>472/mm^2) and low-infiltrated tumors (≤472/mm^2) infiltrated tumors (online supplemental figure 2C) was determined. Within the stroma, the median CD163+ cells density was 1395 cells/mm^2 (126–6235) and the cut-off value to define high-infiltrated tumors (>1350/mm^2) and low-infiltrated tumors (≤1350/mm^2) infiltrated tumors was 1350 cells/mm^2 (online supplemental figure 2D). A high level of stroma CD8+ cell infiltration was significantly associated with improved outcome (figure 1B–D) whereas we found only a non-significant trend for intratumoral CD8+ infiltration (online supplemental figure 3A–C). Interestingly, we found a statistically significant correlation between low intratumoral CD163+ cell infiltration and improvement of clinical benefit rate (p=0.05), PFS (HR=0.61, 95% CI 0.4 to 0.94, p=0.023), and OS (HR=0.48, 95% CI 0.29 to 0.8, p=0.004) under ICB therapy (figure 1E–G) whereas within the stroma, CD163 infiltration was not significantly associated with survival (online supplemental figure 3D–F) thus highlighting the importance of spatial distribution of immune cells to determine clinical outcome. On multivariate analysis, tumor CD163+ cell infiltration remained independently associated with both PFS and OS (table 2).

CD163+ cell infiltration is associated with PD-L1 expression

We then analyzed the correlation between PD-L1 expression (online supplemental figure 4A) scores and CD163+ cell infiltration. The level of macrophage infiltration was higher in tumors with a PD-L1 TPS ≥1% than in PD-L1-negative tumors (median density: 1693 vs 906, p=0.025,

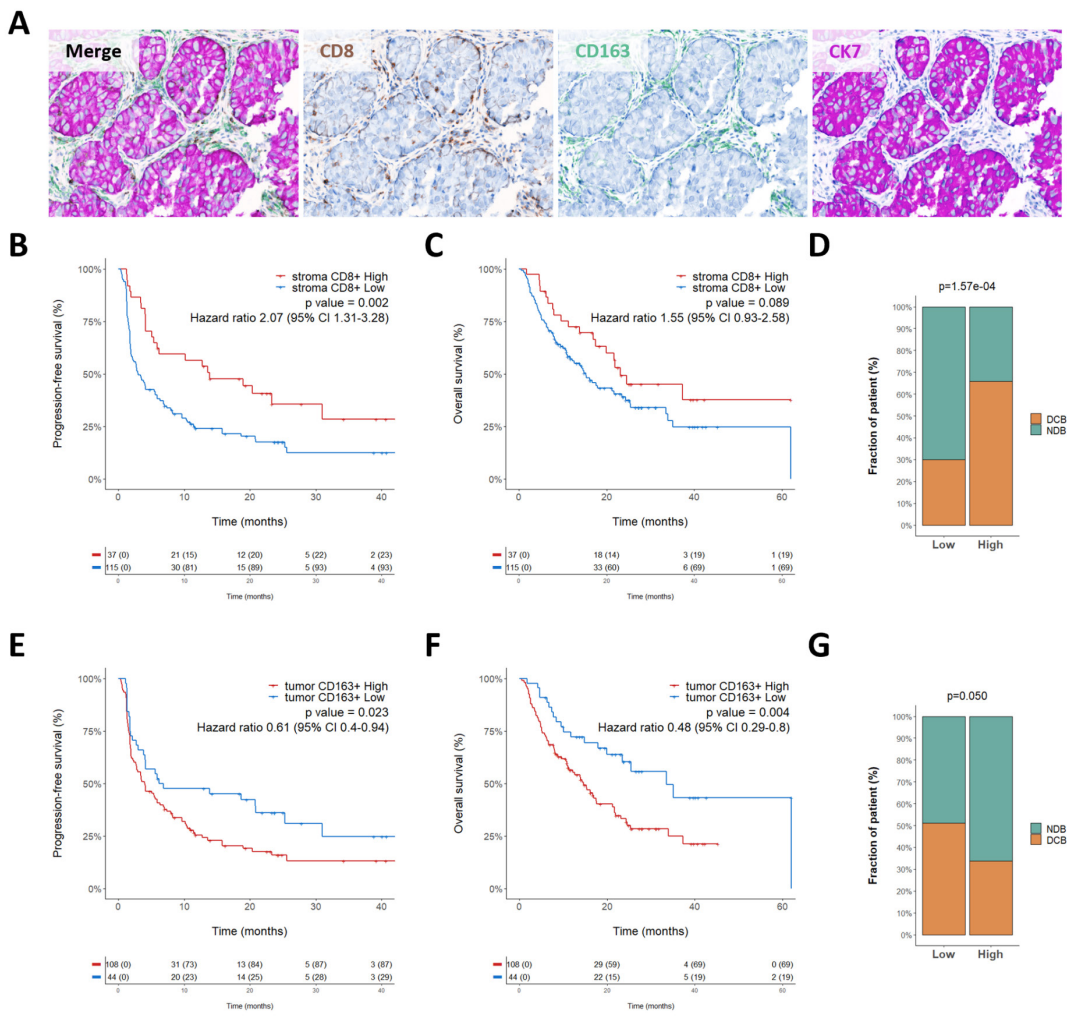

Figure 1 CD163+ cell tumor infiltration is correlated with poor clinical outcome. (A) Representative images of lung cancer sample stained with the multiplexed panel CD8/CD163/CK7—Objective 20× (B–C) Kaplan-Meier curves of progression-free survival (B) and overall survival (C) according to stroma CD8+ cell density. (D) Proportion of patients who experienced durable clinical benefit (DCB) or non-clinical benefit (NCB) according to their level of CD8+ stroma infiltration classified as high and low. P value was calculated using χ^2 test.(E–F) Kaplan-Meier curves of progression-free survival (E) and overall survival (F) according to tumor CD163 +cell density. (G) Proportion of patients who experienced DCB or NCB according to their level of CD163+ tumor infiltration classified as high and low. P value was calculated using χ^2 test.

online supplemental figure 4B). Regardless of the PD-L1 expression status, patients with a low CD163+ cell density had better outcomes. Among patients with PD-L1-positive tumors (ie, TPS ≥1%) and PD-L1-negative tumors (ie, TPS <1%), the clinical benefit rates in patients with a low CD163+ cell density were 77% and 39%, respectively (p=0.047), versus 46% and 22%, respectively (p=0.1), in patients with high CD163 +cell density (online supplemental figure 4E–H).

Among patients with a PD-L1 TPS ≥1%, the median PFS and OS were, respectively, 30.9 (95% CI 18.69 to NA) and 62 (95% CI NA to NA) months in the low CD163+ cell density group versus 5.08 (95% CI 1.93 to 12.8) and 16.2 (95% CI 11.3 to NA) months in the high CD163+ cell density; overall log-rank test p=0.016 (PFS) and p=0.008 (OS) (online supplemental figure 4C,D). Among patients with a PD-L1 TPS <1%, the median PFS and OS were, respectively, 5.0 (95% CI 1.8 to 25.34) and 25.5 (95% CI 14.85 to NA) months in the low CD163+ cell density group versus 3.4 (95% CI 2.2 to 6.85) and 12.7 (95% CI 8.16 to 23.1) months in the high CD163+ cell density group; overall log-rank test p=0.112 (PFS) and p=0.028 (OS) (online supplemental figure 4F,G).

Gene expression features in tumor compartment associated with macrophage infiltration

To decipher the determinants of macrophage infiltration in patients with NSCLC, we spatially profiled the expression of 78 transcripts in situ across 16 tumor specimens (eight each with low and high macrophage infiltration) using the NanoString GeoMx Immune Pathway Assay.[13] We first stained tumor sections with markers for immune (CD45) and epithelial (PanCK) compartments to separately profile RNA from the stroma (PanCK–) and tumor

Table 1 Main characteristics of patients (n=152)

Characteristic	n (%)
Median age (range)	62 (30–92)
Gender	
Female	58 (38)
Male	94 (62)
Performance status	
ECOG 0 & 1	127 (84)
ECOG ≥2	25 (16)
Stage IV cancer	152 (100)
Immunotherapy	
Anti PD1/PD-L1 monotherapy	137 (90)
Anti PD1/PD-L1 in combination with another ICI	15 (10)
Histology	
Adenocarcinoma	149 (98)
Other	3 (2)
PD-L1 expression	
High (≥1%)	64 (42)
Low (<1%)	85 (56)
Not evaluable	3 (2)
MSI status	
MSS	62 (41)
MSI-high	2 (1)
Unknown	88 (58)
Previous lines of treatment	
≤1	93 (61)
>1	20 (13)
Missing	39 (26)
Best response to ICI (RECIST V.1.1)	
OR	51 (33)
SD	36 (24)
PD	58 (38)
Unknown	7 (5)

ECOG, The Easter Cooperative Oncology Group; ICI, immune checkpoint inhibitor; MSI, microsatellite instability; MSS, microsatellite stable; OR, objective response; PD1, programmed cell death 1; PD, progression disease; PD-L1, programmed death-ligand 1; RECIST, Response Evaluation Criteria in Solid Tumors; SD, stable disease.

areas (PanCK+/CD45−) (figure 2A). Analysis of the expression of the PTPRC (CD45) and PanCK (multiple cytokeratin genes) genes in each compartment illustrated the good segmentation of both areas (figure 2B). A total number of 381 spatially distinct areas (11–12 ROIs per patient) were finally analyzed on the GeoMX platform.

Unsupervised hierarchical clustering analysis demonstrated that the tumor ROIs data set allowed for accurate distinction between patients with high and low CD163+ infiltration (figure 2C). We focused then on this data set to explore the possible determinants involved in the homing of macrophage within the tumor. Analysis of the tumorous compartment revealed that three genes were significantly upregulated in tumors associated with high macrophage infiltration. These included genes encoding for integrin (*ITGAM (CD11b)*), chemokine (*CCL5*), and a receptor (*CD27*). On the other hand, two genes were significantly upregulated in low CD163-infiltrated tumors, namely the anti-apoptotic factor (*BCL2*) and the antigen-presenting molecule *HLA-E* (figure 2D and online supplemental table 2). Interestingly, analysis of the stroma compartment revealed a significant upregulation of *BCL2* expression in low macrophage-infiltrated tumors (online supplemental figure 5).

To confirm these data, we analyzed the correlation between the level of CD163+ cell infiltration, as determined through IHC, and expression of these genes evaluated by bulk RNAseq of 29 cases (figure 2E and online supplemental figure 6). We confirmed the significant positive correlation between the expression level of the *ITGAM*, *CCL5*, and *CD27* and the level of macrophage infiltration and the negative correlation with *BCL2*. However, while a negative correlation between HLA-E and CD163 infiltration level was depicted using the spatial transcriptomics approach, results obtained through bulk RNAseq gave an opposite trend, thus suggesting the importance of spatial profiling to correlate gene expression with microenvironment features.

Gene expression features of TAMs and correlation with response to ICBs

Although we found that high intratumoral macrophage infiltration was associated with poor outcomes on ICB, some patients with highly macrophages-infiltrated tumors showed a good response. To decipher the determinants of response in patients with NSCLC with high macrophage infiltration, we spatially profiled the expression of 78 transcripts in situ across eight tumors with high macrophage infiltration (four each with objective response and progressive disease) by using the NanoString GeoMx Immune Pathway Assay as described above. Unsupervised hierarchical clustering analysis demonstrated that the stroma ROIs data set allowed for a good distinction between responders and non-responders (figure 3A). Analysis of the stroma compartment revealed that 10 genes were differentially expressed between responders and non-responders (online supplemental table 3 and figure 3B). Among them, four genes were associated with the IFN-γ signaling pathway (*STAT1, CD44, IFNGR1,* and *HLA-E*). Similarly, three genes associated with the M1 phenotype including *STAT1, CD44* and *LY6E* were significantly upregulated in responders, whereas the *BCL2* gene associated with the M2 phenotype was significantly upregulated in non-responders.[17–20]

Surprisingly, we found a significantly higher expression of *CSF1R* in responders versus non-responders in the stroma compartment (figure 3B, online supplemental

Table 2 Multivariate analysis for progression-free and overall survival

Endpoint	Subgroup	N	HR	95% CI	P value
PFS	PD-L1 status (TPS ≥1)	n 110	0.54	(0.33 to 0.87)	0.012
	Stromal CD8+ (>697)		0.59	(0.34 to 1.01)	0.055
	Sex (male)		0.87	(0.54 to 1.39)	0.560
	Age (>62)		1.04	(0.65 to 1.65)	0.868
	Intratumoral CD163+ (>472 cells/mm^2)		1.80	(1.10 to 2.93)	0.019
	Previous treatment line (>1)		1.82	(1.05 to 3.15)	0.034
	Performance status (>1)		1.96	(1.07 to 3.59)	0.030

Continued

Table 2 Continued

Endpoint	Subgroup	N		HR	95% CI	P value
OS	PD-L1 status (TPS ≥1)	110		0.50	(0.27 to 0.92)	0.027
	Stromal CD8+ (>697)			0.68	(0.36 to 1.28)	0.233
	Sex (male)			0.72	(0.41 to 1.29)	0.276
	Age (>62)			1.33	(0.77 to 2.31)	0.308
	Previous treatment line (>1)			2.05	(1.10 to 3.80)	0.023
	Intratumoral CD163+ (>472 cells/mm^2)			2.69	(1.45 to 4.99)	0.002
	Performance status (>1)			3.82	(1.92 to 7.60)	<0.001

OS, overall survival; PD-L1, programmed cell death ligand 1; PFS, progression -free survival; TPS, tumor proportion score .

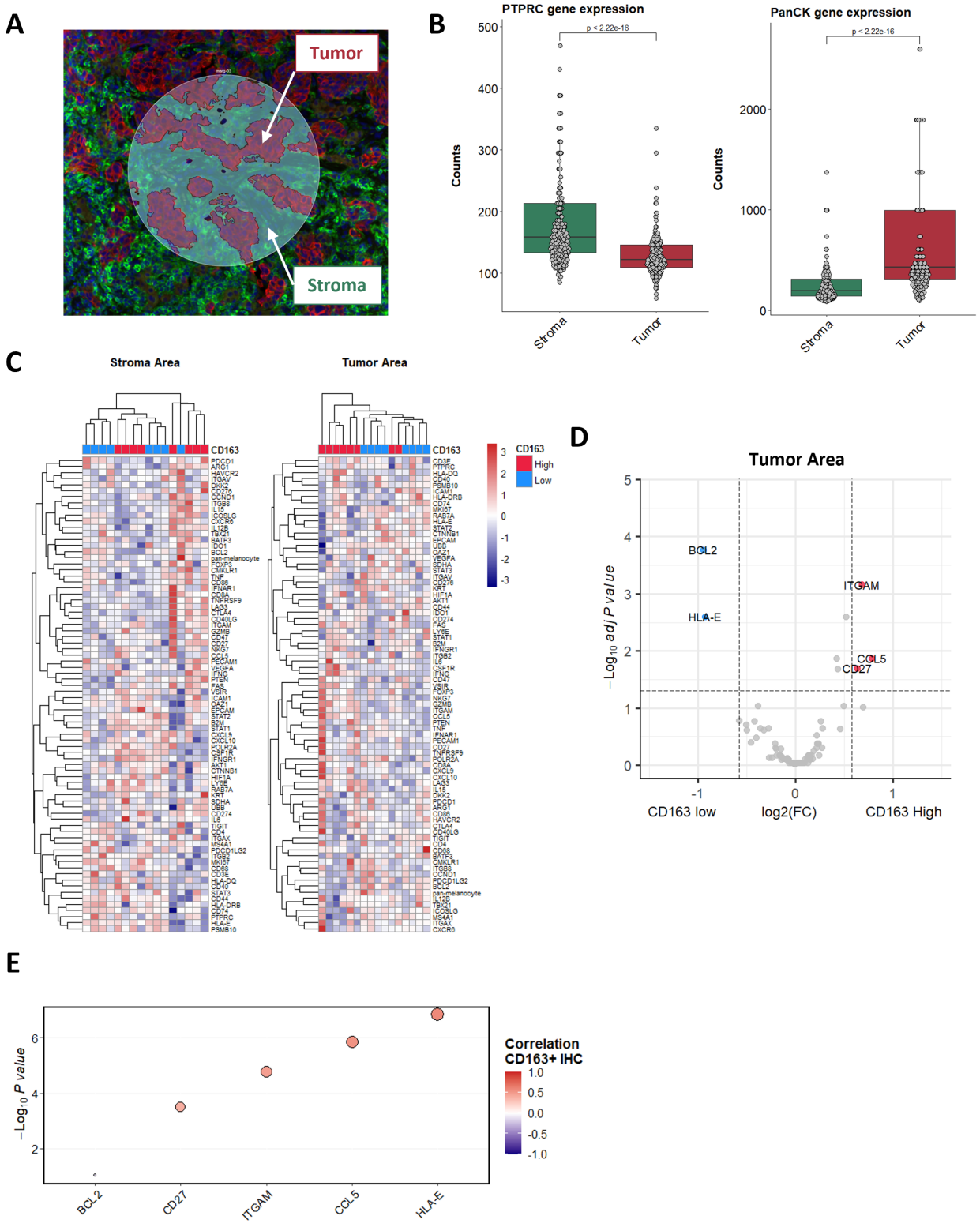

Figure 2 Tumor expression of CCL5 induces CD163+ cell recruitment. (A) Tissue segmentation in tumor (red) and stroma (green) areas of illumination (AOI), performed on the GeoMX DSP platform. (B) Representation of CD45 (left) and PanCK (right) expression in the tumor and stroma AOIs. (C) Unsupervised clustering of tumor patient samples based on the averaged expression of the GeoMX Immune Pathways Panel probes in the tumor and stroma areas. Levels of CD163+ cell infiltration classified as high (red) and low (blue) are annotated. (D) Volcano plot representation of the gene differentially expressed by CD163+ high and low patients in their tumor areas. (**E**) Spearman correlation of the CD163+ cell density determined by IHC and the level of messenger RNA expression of indicated genes assessed by bulk RNA sequencing. DSP, Digital Spatial Profiler; IHC, immunohistochemistry.

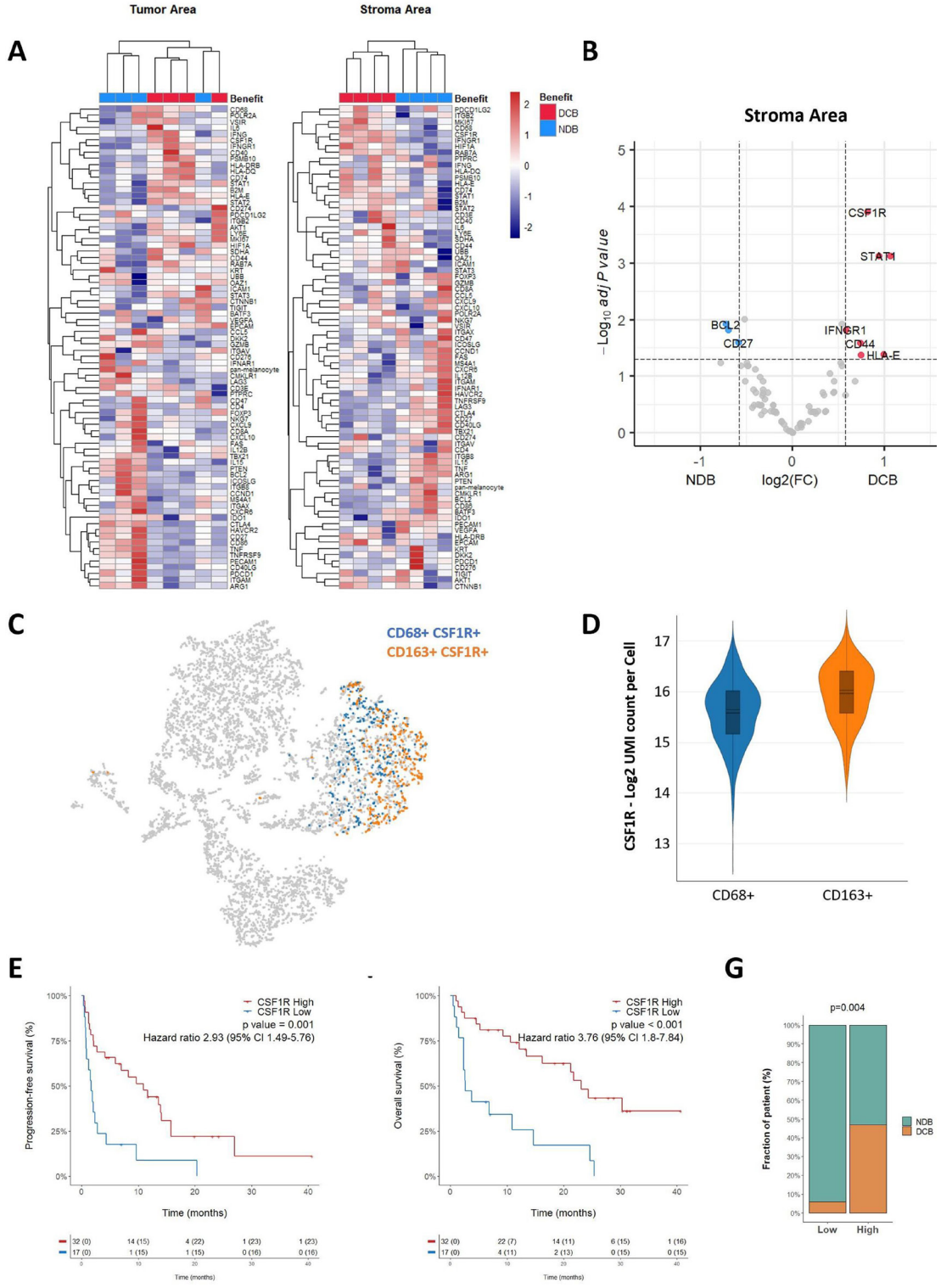

Figure 3 M1-associated genes are enriched in immunotherapy-responsive patients with high level of CD163+ cell infiltration. (A) Unsupervised clustering of patient with tumor samples based on the averaged expression of the GeoMX Immune Pathways Panel probes in the tumor and stroma areas. The patient response classified as non-clinical benefit (NDB—blue) and durable clinical benefit (DCB—red) is annotated. (B) Volcano plot representation of the gene differentially expressed in the stroma areas of patients who experienced DCB and NCB. (C) tSNE visualization of 10× scRNA-seq of non-small cell lung cancer biopsy. Cells co-expressing CD68 or CD163 together with CSF1R are highlighted in blue and orange, respectively. (D) Representation of CSF1R expression in CD68+ and CD163+ cells, as assessed by scRNAseq. (E–F) Kaplan-Meier curves of progression-free survival (E) and overall survival (F) of patients according to the expression of CSF1R determined by RNAseq and classified as high or low. (G) Proportion of patients who experienced DCB or NCB according to their level of CSF1R expression determined by RNAseq and classified as high and low. P value was calculated using χ^2 test. IFN, interferon; RNAseq, RNA sequencing; scRNA -seq, single cell RNAseq. tSNE, t-distributed stochastic neighbor embedding.

figure 7). This gene is mainly associated with the immunosuppressive M2 phenotype. Nevertheless, by exploring a public scRNAseq data set, we found that *CSF1R* was expressed in both CD68+/CD163− and CD68−/CD163+TAMs, suggesting that *CSF1R*-expressing TAMs represent a distinct biological subset (figure 3C,D). To confirm the correlation between *CSF1R* expression and response to ICB, we analyzed the bulk RNAseq data from 49 cases in our cohort for whom genomic data were available. As shown in figure 3, high *CSF1R* expression was associated with an improved DCB rate (47% vs 6%, p=0.004) (figure 3G), PFS (median 10.89 (5.97–15.8) months vs 1.67 (0.92–4.36) months p=0.001) (figure 3E) and OS (median 23.11 (16.2–NA) months vs 2.66 (2.36-NA) months, p<0.001) (figure 3F). To confirm the robustness of our data, we have also analyzed the gene expression data from two other independent data sets including respectively 22 and 21 patients with advanced NSCLC and treated with ICB.[13 14] As shown in online supplemental figure 8, high *CSF1R* gene expression was associated with significantly improved PFS and DCB rate in both data sets. To confirm that *CSF1R* gene expression is predictive of ICB efficacy and has no intrinsic prognostic value, we analyzed the gene expression data from 506 patients who underwent surgery for the treatment of localized NSCLC and who were included in TCGA database. As shown in online supplemental figure 9, *CSF1R* gene expression is not associated with progression free or OS in this cohort confirming that its correlation with outcome is related to treatment with ICB.

DISCUSSION

Apart from the use of the combine positive score, which assesses PD-L1 expression on both tumor and immune cells, the current biomarkers used to tailor immune checkpoint blockade in patients with cancer are related to specific features of tumor cells (PD-L1 expression as assessed by TPS, tumor mutational burden, and microsatellite instability). However, there is growing interest in characterizing the whole TME to identify additional aspects that can help distinguish potential responders from resistant patients. By analyzing pretreatment tumor samples from patients with advanced NSCLC (mainly adenocarcinomas) treated with ICB, we found that tumor compartment enrichment in TAMs is associated with resistance to immunotherapy, regardless of the PD-L1 expression status of tumor cells.

These results are in line with those of a recent study underscoring the potential role of macrophages in the phenomenon of hyperprogression.[21] By analyzing the baseline biopsies of a small cohort of 39 patients with NSCLC, the authors were able to demonstrate an enrichment in CD163+CD33+PD-L1+ macrophages in tumors from hyperprogressor patients in comparison with patients not experiencing hyperprogression.

Besides the level of TAMs infiltration, our results suggest that their spatial distribution play an important role to determine the outcome of patients with NSCLC treated with ICB. Indeed, we did not observe a statistically significant correlation between the level of TAM infiltrating the stroma and patient's outcome. This result is in line with previous studies showing that the prognostic impact of TAMs in NSCLC is directly linked to their distance from tumors cells, the survival of patients being longer among patients with tumor cells that were distant from TAMs.[22]

Although, it is well recognized that TAMs are important modulators of antitumor immunity, the molecular mechanisms that regulate their abundance within the TME remain incompletely clear. To investigate the determinants of macrophage infiltration in NSCLC more in depth, we performed a comparative spatial analysis of the expression of immune genes in tumor samples characterized by a low and high level of macrophage infiltration. We found that *CD27, CCL5,* and *ITGAM* were the three most significantly upregulated genes in tumors characterized by a high level of TAMs infiltration. Our results confirm several preclinical or translational studies showing how the proteins encoded by these genes play a crucial in controlling tumor macrophage polarization and/or recruitment in lung carcinoma or other tumor models and may therefore represent potential innovative immunotherapy targets.[23–26]

TAMs are classically clustered into two major phenotypes, with the dominant group reported to be anti-inflammatory and immune-regulatory and therefore tumor-promoting (also termed M2 macrophages) as opposed to pro-inflammatory and tumoricidal (also termed M1 macrophages). However, this M1/M2 classification is probably too simplistic.[27] There are several lines of evidence suggesting that the macrophages present in the TME reflect a continuum of different phenotypes that cannot be captured solely with the M1/M2 dichotomy.[26 28] To investigate the molecular profile of macrophage infiltration and its correlation with response to ICB in more depth, we performed a spatial analysis of the expression of immune genes in tumor samples characterized by a high level of macrophage infiltration. In both immune (CD45) and tumor (PanCK) compartments, we observed a positive spatial correlation between the expression of genes belonging to the M1 phenotype and the likelihood of response to ICB, whereas M2 genes such as Bcl2 were more highly expressed in patients displaying resistance to treatment.

Unexpectedly, the *CSF1R* gene was the gene most significantly upregulated in patients with high macrophage infiltration and good outcomes on treatment with ICBs. We confirmed this correlation by analyzing the bulk RNAseq data of a cohort of 49 patients with NSCLC treated with ICB. These results were consistent with the findings of Qi *et al* showing that the expression of *CSF1R* is highly predictive of response to anti-PD-1 therapy in NSCLC.[29] Although *CSF1R*-expressing TAMs have been shown to promote tumor progression in several models, their role is controversial in lung cancer. A recent study showed the absence of prognostic impact of high

expression levels of CSF1R in patients with NSCLC who smoke.[30] Another study investigating the effects of anti-CSF1R blockade on solid tumors did not show any effect on tumor growth in several models, including a lung carcinoma model.[31] Overall, the clinical activity observed in clinical trials testing CSF-1/CSF-1R-targeting agents in patients with solid tumors was quite modest despite their demonstrated ability to deplete CSF-1R+CD163+ macrophages.[32 33] Our results showing that high *CSF1R* expression was associated with better outcomes in patients with highly TAM-infiltrated tumors illustrate the complexity of the biology of the CSF1R pathway and its role in the TME. This complexity has recently been illustrated by two seminal studies providing evidence that CSFR1+ TAMs form a partially redundant cellular network with Foxp3+ Treg cells and myeloid-derived suppressor cells which may modulate sensitivity to immunotherapy.[34 35]

Altogether, our results based on the comprehensive analysis of tumor samples from patients with NSCLC treated with ICBs demonstrate the deleterious impact of intratumoral TAM infiltration and identify new potential targets to alter TAM polarization and/or recruitment. Our data also suggest that CSF1R inhibition may not be an appropriate strategy to target macrophages and improve ICB efficacy and that other approaches should be explored to limit their pro-tumorigenic roles.

Author affiliations
[1]Department of Medecine, Institut Bergonié, Bordeaux, France
[2]Faculty of Medecine, University of Bordeaux, Bordeaux, France
[3]Explicyte Immuno-Oncology, Bordeaux, France
[4]Department of Medecine, Gustave Roussy, Villejuif, France
[5]Department of Oncology, Clinique Marzet, Pau, France
[6]Department of Pathology, Institut Bergonié, Bordeaux, France
[7]Department of Pathology, Gustave Roussy, Villejuif, France
[8]DITEP, Gustave Roussy, Villejuif, France

Twitter Mathieu Larroquette @MathieuLrqt

Contributors AI and AB conceived and designed the study. FLL and IS performed the histological analyses. BB, SC, J-CS, FB, AI provided study material or treated patients. All authors collected and assembled data. AI, J-PG, AB, ML developed the tables and figures. AI, ML, J-PG, AB conducted the literature search and wrote the manuscript. All authors were involved in the critical review of the manuscript and approved the final version. AI accepts full responsibility for the work and/or the conduct of the study, had access to the data, and controlled the decision to publish.

Funding Institut Bergonie and Explicyte.

Competing interests ML, IS, SC, FLL: Nothing to disclose. AB, J-PG, CR: Employees of Explicyte. AI: Received research grants from AstraZeneca, Bayer, BMS, Chugai, Merck, MSD, Pharmamar, Novartis, Roche, and received personal fees from Epizyme, Bayer, Lilly, Roche, and Springworks. BB: Received grants from AstraZeneca, Pfizer, Eli Lilly, Onxeo, Bristol Myers Squibb, Inivata, AbbVie, Amgen, Blueprint Medicines, Celgene, GlaxoSmithKline, Ignyta, Ipsen, Merck KGaA, MSD Oncology, Nektar, PharmaMar, Sanofi, Spectrum Pharmaceuticals, Takeda, Tiziana Therapeutics, Cristal Therapeutics, Daiichi Sankyo, Janssen Oncology, OSE Immunotherapeutics, BeiGene, Boehringer Ingelheim, Genentech, Servier, Tolero Pharmaceuticals. J-CS: Has received consultancy fees from AstraZeneca, Astex, Clovis, GSK, GamaMabs, Lilly, MSD, Mission Therapeutics, Merus, Pfizer, Pharma Mar, Pierre Fabre, Roche/Genentech, Sanofi, Servier, Symphogen, and Takeda. FB: Has received consultancy fees from AstraZeneca, Astex, Clovis, GSK, GamaMabs, Lilly, MSD, Mission Therapeutics, Merus, Pfizer, Pharma Mar, Pierre Fabre, Roche/Genentech, Sanofi, Servier, Symphogen, and Takeda.

Patient consent for publication Not applicable.

Ethics approval This study involves human participants and was approved by IRB Institut Bergonié and IRB Gustave Roussy. Participants gave informed consent to participate in the study before taking part.

Provenance and peer review Not commissioned; externally peer reviewed.

Data availability statement Data are available upon reasonable request to the corresponding author.

ORCID iD
Antoine Italiano http://orcid.org/0000-0002-8540-5351

REFERENCES

1 Vaddepally RK, Kharel P, Pandey R, *et al*. Review of indications of FDA-approved immune checkpoint inhibitors per NCCN guidelines with the level of evidence. *Cancers* 2020;12:E738.
2 Doroshow DB, Sanmamed MF, Hastings K, *et al*. Immunotherapy in non-small cell lung cancer: facts and hopes. *Clin Cancer Res* 2019;25:4592–602.
3 Prelaj A, Tay R, Ferrara R, *et al*. Predictive biomarkers of response for immune checkpoint inhibitors in non-small-cell lung cancer. *Eur J Cancer* 2019;106:144–59.
4 Davis AA, Patel VG. The role of PD-L1 expression as a predictive biomarker: an analysis of all US food and drug administration (FDA) approvals of immune checkpoint inhibitors. *J Immunother Cancer* 2019;7:278.
5 Zhang Q-wen, Liu L, Gong C-yang, *et al*. Prognostic significance of tumor-associated macrophages in solid tumor: a meta-analysis of the literature. *PLoS One* 2012;7:e50946.
6 Gentles AJ, Newman AM, Liu CL, *et al*. The prognostic landscape of genes and infiltrating immune cells across human cancers. *Nat Med* 2015;21:938–45.
7 DeNardo DG, Ruffell B. Macrophages as regulators of tumour immunity and immunotherapy. *Nat Rev Immunol* 2019;19:369–82.
8 Vitale I, Manic G, Coussens LM, *et al*. Macrophages and metabolism in the tumor microenvironment. *Cell Metab* 2019;30:36–50.
9 Cassetta L, Fragkogianni S, Sims AH, *et al*. Human tumor-associated macrophage and monocyte transcriptional landscapes reveal cancer-specific reprogramming, biomarkers, and therapeutic targets. *Cancer Cell* 2019;35:588–602.
10 Sharma P, Hu-Lieskovan S, Wargo JA, *et al*. Primary, adaptive, and acquired resistance to cancer immunotherapy. *Cell* 2017;168:707–23.
11 Planchard D, Popat S, Kerr K, *et al*. Metastatic non-small cell lung cancer: ESMO clinical practice guidelines for diagnosis, treatment and follow-up. *Ann Oncol* 2018;29:iv192–237.
12 Eisenhauer EA, Therasse P, Bogaerts J, *et al*. New response evaluation criteria in solid tumours: revised RECIST guideline (version 1.1). *Eur J Cancer* 2009;45:228–47.
13 Merritt CR, Ong GT, Church SE, *et al*. Multiplex digital spatial profiling of proteins and RNA in fixed tissue. *Nat Biotechnol* 2020;38:586–99.
14 Loriot Y, Marabelle A, Guégan JP, *et al*. Plasma proteomics identifies leukemia inhibitory factor (LIF) as a novel predictive biomarker of immune-checkpoint blockade resistance. *Ann Oncol* 2021;32:1381–90.
15 Prat A, Navarro A, Paré L, *et al*. Immune-related gene expression profiling after PD-1 blockade in non-small cell lung carcinoma, head and neck squamous cell carcinoma, and melanoma. *Cancer Res* 2017;77:3540–50.
16 Hwang S, Kwon A-Y, Jeong J-Y, *et al*. Immune gene signatures for predicting durable clinical benefit of anti-PD-1 immunotherapy in patients with non-small cell lung cancer. *Sci Rep* 2020;10:643.

17 Orecchioni M, Ghosheh Y, Pramod AB, *et al*. Macrophage polarization: different gene signatures in M1(LPS+) vs. classically and M2(LPS-) vs. alternatively activated macrophages. *Front Immunol* 2019;10:1084.
18 Di Martile M, Farini V, Consonni FM, *et al*. Melanoma-specific Bcl-2 promotes a protumoral M2-like phenotype by tumor-associated macrophages. *J Immunother Cancer* 2020;8:e000489.
19 Liu LF, Kodama K, Wei K, *et al*. The receptor CD44 is associated with systemic insulin resistance and proinflammatory macrophages in human adipose tissue. *Diabetologia* 2015;58:1579–86.
20 Li C, Menoret A, Farragher C, *et al*. Single cell transcriptomics based-MacSpectrum reveals novel macrophage activation signatures in diseases. *JCI Insight* 2019;5:126453.
21 Lo Russo G, Moro M, Sommariva M, *et al*. Antibody-Fc/FcR interaction on macrophages as a mechanism for Hyperprogressive disease in non-small cell lung cancer subsequent to PD-1/PD-L1 blockade. *Clin Cancer Res* 2019;25:989–99.
22 Zheng X, Weigert A, Reu S, *et al*. Spatial density and distribution of tumor-associated macrophages predict survival in non-small cell lung carcinoma. *Cancer Res* 2020;80:4414–25.
23 Perea F, Bernal M, Sánchez-Palencia A, *et al*. The absence of HLA class I expression in non-small cell lung cancer correlates with the tumor tissue structure and the pattern of T cell infiltration. *Int J Cancer* 2017;140:888–99.
24 Turaj AH, Hussain K, Cox KL, *et al*. Antibody tumor targeting is enhanced by CD27 agonists through myeloid recruitment. *Cancer Cell* 2017;32:777–91.
25 Schmid MC, Khan SQ, Kaneda MM, *et al*. Integrin CD11b activation drives anti-tumor innate immunity. *Nat Commun* 2018;9:5379.
26 Aldinucci D, Borghese C, Casagrande N. The CCL5/CCR5 axis in cancer progression. *Cancers* 2020;12:E1765.
27 Mantovani A, Sozzani S, Locati M, *et al*. Macrophage polarization: tumor-associated macrophages as a paradigm for polarized M2 mononuclear phagocytes. *Trends Immunol* 2002;23:549–55.
28 DeNardo DG, Ruffell B. Macrophages as regulators of tumour immunity and immunotherapy. *Nat Rev Immunol* 2019;19:369–82.
29 Qi X, Qi C, Wu T, *et al*. CSF1R and HCST: novel candidate biomarkers predicting the response to immunotherapy in non-small cell lung cancer. *Technol Cancer Res Treat* 2020;19:153303382097066.
30 Inamura K, Shigematsu Y, Ninomiya H, *et al*. CSF1R-expressing tumor-associated macrophages, smoking and survival in lung adenocarcinoma: analyses using quantitative Phosphor-Integrated dot staining. *Cancers* 2018;10:E252.
31 O'Brien SA, Orf J, Skrzypczynska KM, *et al*. Activity of tumor-associated macrophage depletion by CSF1R blockade is highly dependent on the tumor model and timing of treatment. *Cancer Immunol Immunother* 2021;70:2401–10.
32 Gomez-Roca CA, Italiano A, Le Tourneau C, *et al*. Phase I study of emactuzumab single agent or in combination with paclitaxel in patients with advanced/metastatic solid tumors reveals depletion of immunosuppressive M2-like macrophages. *Ann Oncol* 2019;30:1381–92.
33 Papadopoulos KP, Gluck L, Martin LP, *et al*. First-in-human study of AMG 820, a monoclonal anti-colony-stimulating factor 1 receptor antibody, in patients with advanced solid tumors. *Clin Cancer Res* 2017;23:5703–10.
34 Gyori D, Lim EL, Grant FM, *et al*. Compensation between CSF1R+ macrophages and Foxp3+ Treg cells drives resistance to tumor immunotherapy. *JCI Insight* 2018;3:120631.
35 Beffinger M, Tallón de Lara P, Tugues S, *et al*. CSF1R-dependent myeloid cells are required for NK-mediated control of metastasis. *JCI Insight* 2018;3:97792.

SUPPLEMENTARY TABLES AND FIGURES

Supplementary Table 1. Main characteristics of patients included in the MATCH-R study (n=49).

Characteristic	**n (%)**
Median age (range)	64 (32-89)
Gender	
Female	18 (37)
Male	31 (73)
Performance status	
ECOG 0 & 1	40 (82)
ECOG ≥ 2	9 (18)
Stage IV Cancer	49 (100)
Immunotherapy	
Anti PD1 monotherapy	42 (86)
Anti PD-L1 monotherapy	7 (14)
Histology	
Adenocarcinoma	39 (80)
Other	10 (20)
Best response to ICI (RECIST 1.1)	
OR	13(27)
SD	13 (27)
PD	23 (46)

Supplementary Table 2. Genes significantly differentially expressed in NSCLC with high CD163+ TAM infiltration versus low CD163+ TAM infiltration		
Gene symbol	**Fold change**	**Adjusted p value**
Genes upregulated in NSCLC with high CD163+ TAM infiltration		
ITGAM	0,680436	6,89E-04
CCL5	0,781225	0.013
CD27	0,628748	0.02
Genes upregulated in NSCLC with low CD163+ TAM infiltration		
BCL2	-0,94836	1.7E-04
HLA-E	-0,92939	2.5E-03

Supplementary Table 3. Genes with significant differential expression in the stroma compartment of NSCLC with high CD163+ TAM infiltration between responders and non-responders to ICB

Gene symbol	Log Fold change	Adjusted p value
Genes upregulated in responders to ICB		
CSF1R	0,819299	1.26E-04
STAT1	0,941207	7.47E-04
LY6E	1,062774	7.47E-04
IFNGR1	0,583992	0.015
CD44	0,742013	0.026
HLA-E	0,991334	0.042
HLA-DQ	0,744943	0.043
Genes upregulated in non-responders to ICB		
BCL2	-0,72281	0.012
ITGB8	-0,69637	0.015
CD27	-0,58429	0.026

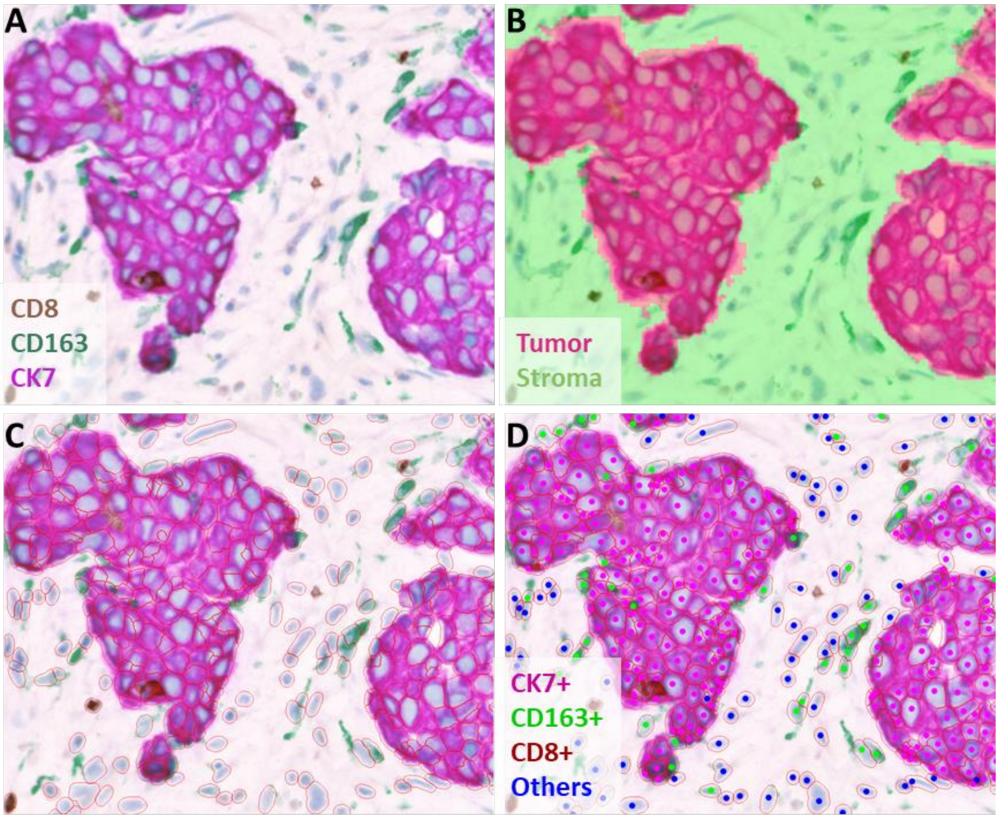

Supplementary figure 1: Immunohistochemistry analysis workflow. Slides were stained with the panel CD8/CD163/CK7 **(A)** and analyzed in Inform to segment the tissue (**B)** in Tumor (red) and Stroma (green) areas. **(C)** Slides were further segmented in cells (red line) based on the hematoxylin counterstaining. **(D)** Cell were finally classified as CK7+, CD8+, CD163+ or others.

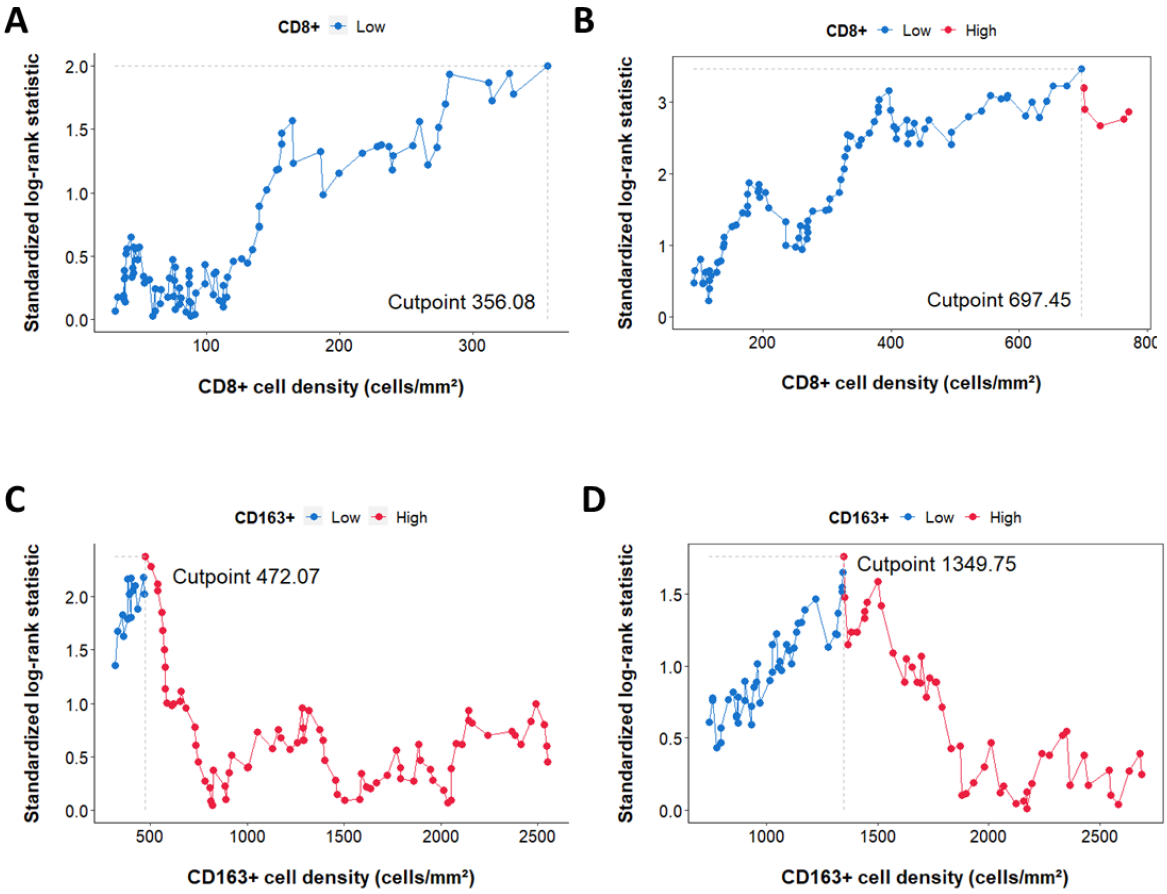

Supplementary figure 2: **IHC staining defined high and low-infiltrated tumors with CD8+ and CD163+ cells**. Using maximally selected rank statistic, cut-off value were determined for intratumoral CD8+ **(A)**, stromal CD8+ **(B)**, intratumoral CD163+ **(C)** and stromal CD163+ **(D)** cell density to define high and low-infiltrated tumours.

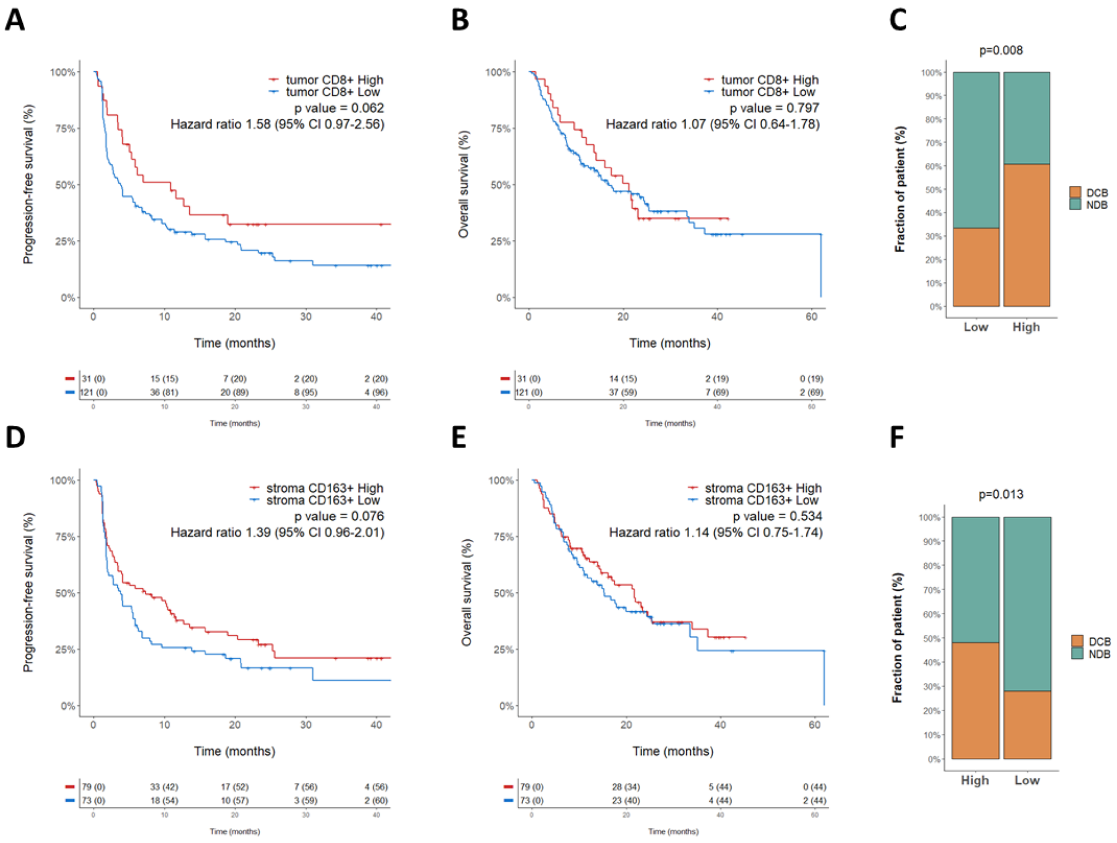

Supplementary figure 3: Correlation of tumor infiltration of CD8+ and of stroma CD163+ cells density with outcome on immunotherapy in patients with NSCLC. (A-B) Kaplan Meier curves of progression-free survival (B) and overall survival (C) according to tumor CD8+ cell density. **(C)** Proportion of patients who experienced durable clinical benefit (DCB) or non-clinical benefit (NCB) according to their level of CD8+ tumor infiltration classified as High and Low. P value is derived from Chi² test **(D-E)** Kaplan Meier curves of progression-free survival (E) and overall survival (F) according to stroma CD163+ cell density. **(F)** Proportion of patients who experienced durable clinical benefit (DCB) or non-clinical benefit (NCB) according to their level of CD163+ stroma infiltration classified as High and Low. P value is derived from Chi² test

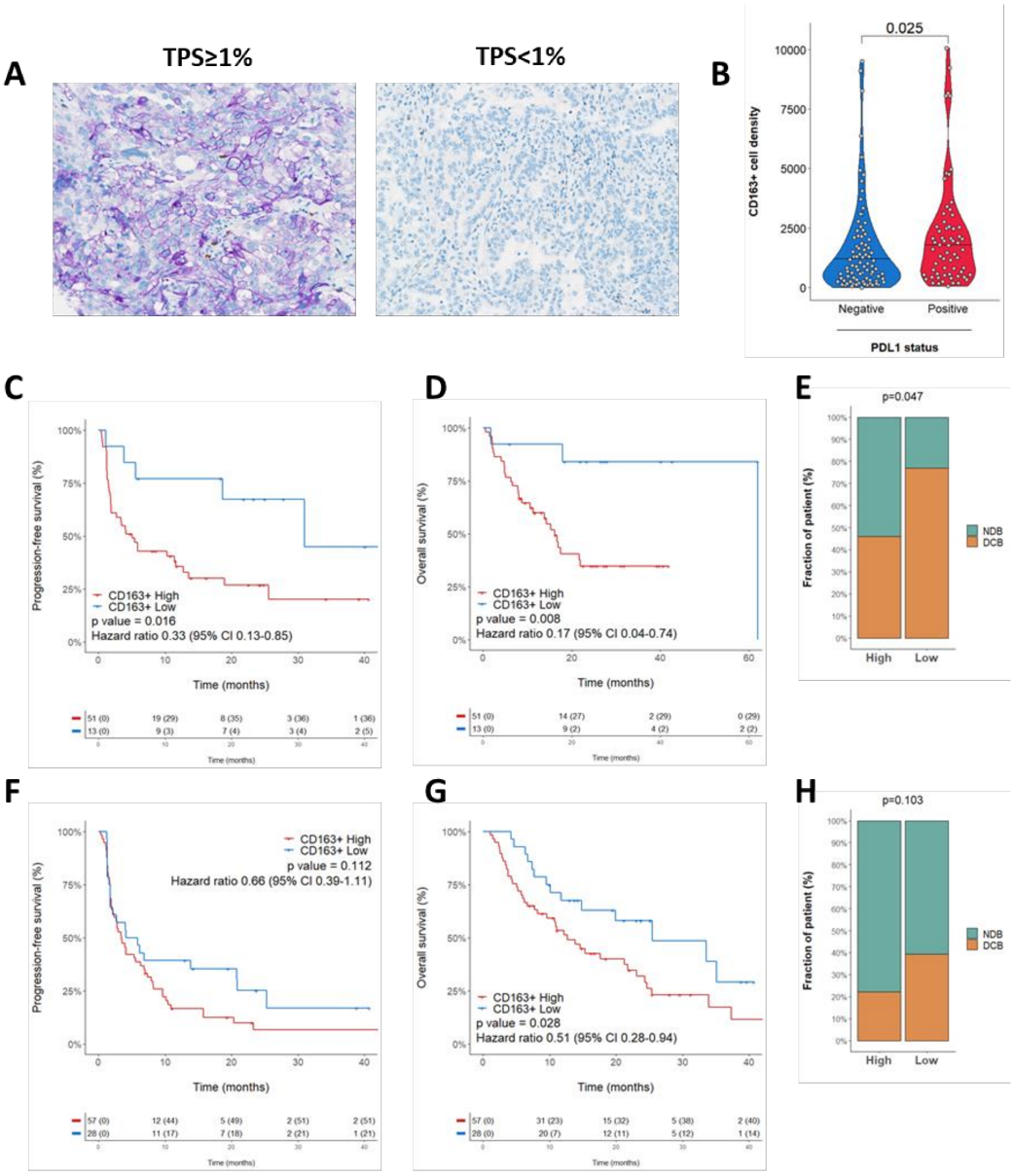

Supplementary figure 4: CD163+ cell infiltration is associated with PDL1 expression status. (A) PDL1 expression was assessed by immunohistochemistry (PDL1 stained in purple). Illustrations here depict tumor cases with negative (TPS<1%) and positive (TPS ≥ 1%) PDL1 expression. (B) Representation of CD163+ cell density in patients according to their PDL1 TPS score (negative = TPS<1 vs positive = TPS ≥1). p value was calculated using Wilcoxon Rank sum test. (C-D) Kaplan Meier curves of progression-free survival (C) and overall survival (D) of PDL1 positive patients according to the tumor CD163+ cell density. (E) Proportion of PDL1 positive patients who experienced durable clinical benefit (DCB) or non-clinical benefit (NCB) according to their level of CD163+ tumor infiltration classified as High and Low. p value was calculated using chi² test. (F-G) Kaplan Meier curves of progression-free survival (F) and overall survival (G) of PDL1 negative patients according to the tumor CD163+ cell density. (H) Proportion of PDL1 negative patients who experienced durable clinical benefit (DCB) or non-clinical

benefit (NCB) according to their level of CD163+ tumor infiltration classified as High and Low. p value was calculated using chi² test.

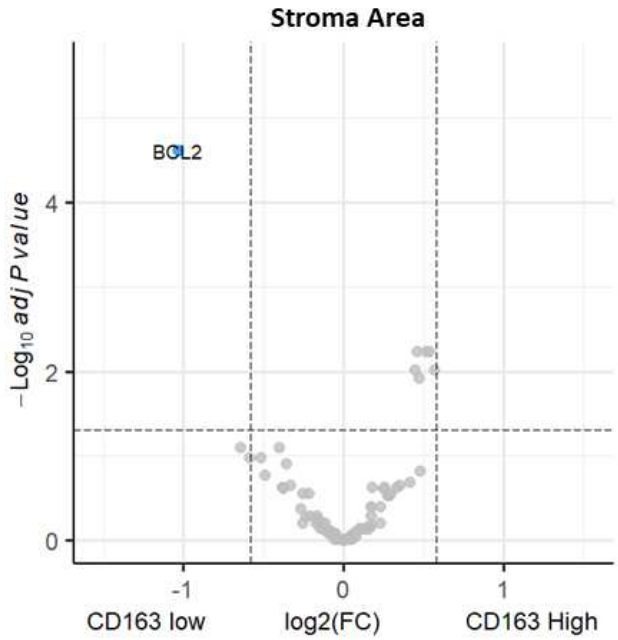

Supplementary figure 5: **Volcano plot representation of genes differentially expressed in the stroma of CD163+ high versus low patients.**

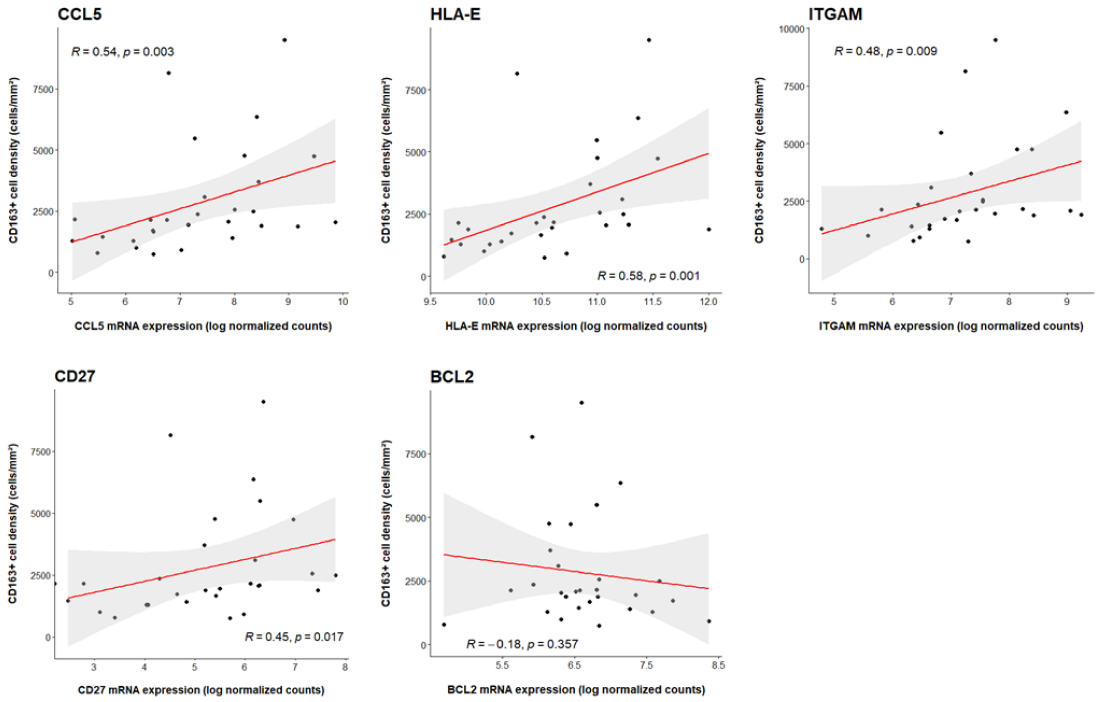

Supplementary figure 6: Spearman correlation of the CD163+ cell density determined by IHC and the level of mRNA expression of indicated genes assessed by RNAseq.

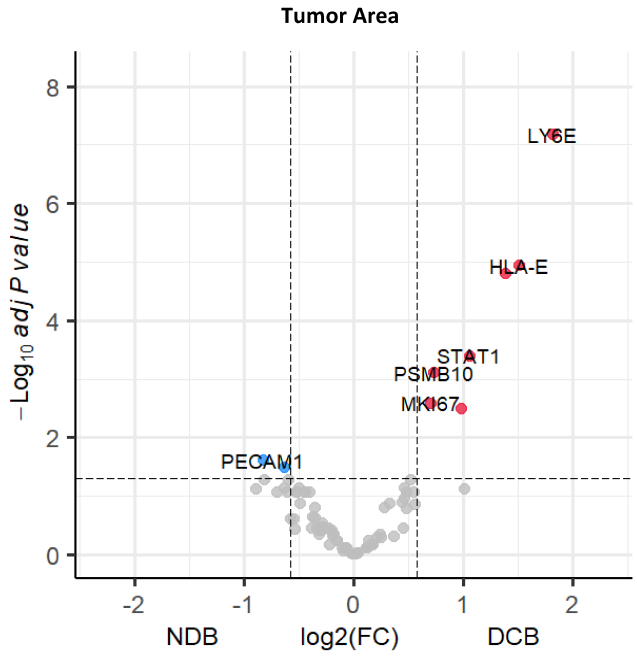

Supplementary figure 7: Volcano plot representation of gene differentially expressed in the tumor of CD163+ high responders versus non-responders patients.

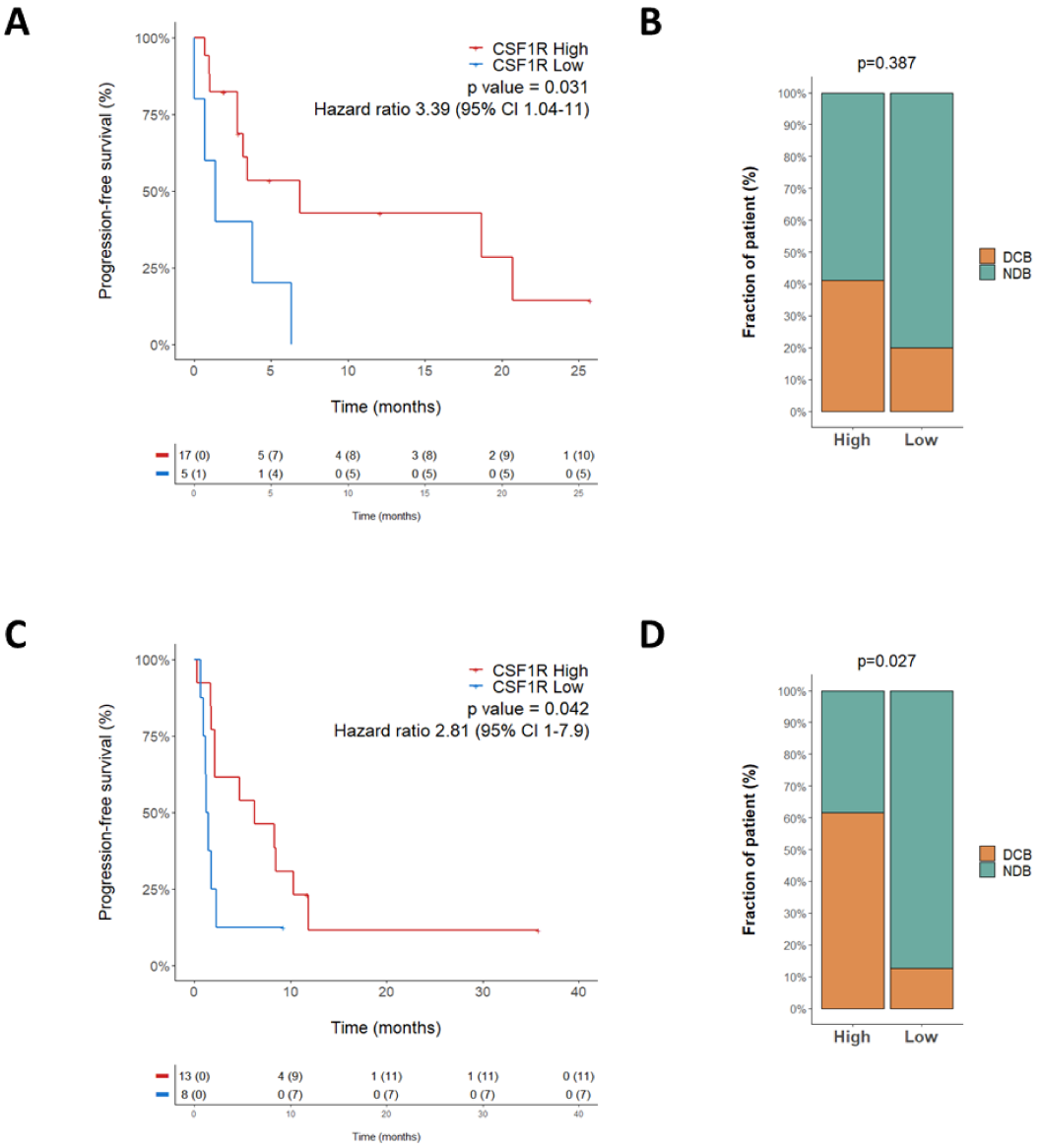

Supplementary Figure 8. Impact of CSF1R expression on anti-PD1 efficacy in patients with advanced NSCLC. (A-B) Analysis from the GSE93157 dataset. (A) Kaplan Meier curve of progression-free survival of patients according to the expression of CSF1R assessed by the nCounter system and classified as High or Low. (B) Proportion of patients who experienced durable clinical benefit (DCB) or non-clinical benefit (NCB) according to their level of CSF1R expression classified as High and Low. p value was calculated using chi² test. (C-D) Analysis from the GSE136961 dataset. (A) Kaplan Meier curve of progression-free survival of patients according to the expression of CSF1R assessed by Ion Torrent system and classified as High or Low. (B) Proportion of patients who experienced durable clinical benefit (DCB) or non-clinical benefit (NCB) according to their level of CSF1R expression classified as High and Low. p value was calculated using chi² test.

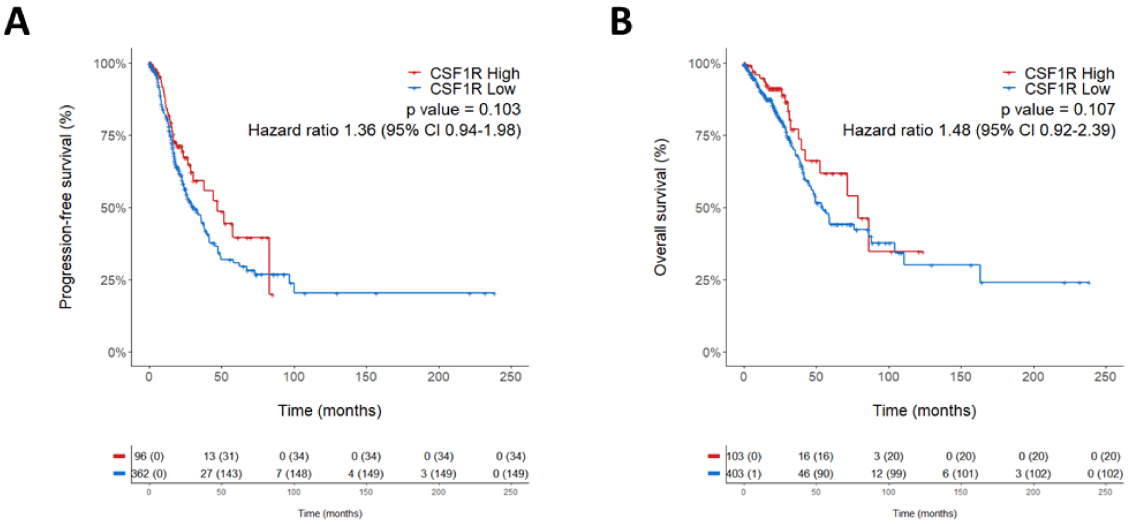

Supplementary Figure 9: Impact of CSF1R expression on progression-free and overall survival in the LUAD TCGA dataset. (A) Kaplan Meier curves of progression-free survival (A) and overall survival (B) of patients with NSCLC according to the expression of *CSF1R* determined by RNAseq and classified as High or Low.